Numerical investigation of flash flood dynamics due to cascading failures of natural landslide dams

Qingyuan Yang[1,2], Mingfu Guan[1*], Yong Peng[3], and Huayong Chen[4]

[1] Department of Civil Engineering, University of Hong Kong, Hong Kong SAR, China.
[2] Department of Hydraulics, Changjiang River Scientific Research Institute, Wuhan, China.
[3] State Key Laboratory of Hydraulics and Mountain River Engineering, Sichuan University, Chengdu, China.
[4] Key Laboratory of Mountain Hazards and Earth Surface Process, Chinese Academy of Science, Chengdu, China.

ABSTRACT: A series of natural landslide dams commonly form in a river valley in mountainous areas. Their failures are frequently triggered by intense rainfall, which may result in severe flash flooding or debris flow in a short period. It is important for risk mitigation to develop greater evidence-based understanding of flood dynamics due to cascading dam failures. Based on detailed hydro-morphodynamic modeling of various scenarios, this study systematically evaluates the formation and evolution of flash floods due to a cascading failure of natural landslide dams. The hydro-morphodynamic model has been shown to be capable of simulating shock-captured flows and resultant morphological changes. In this study, we first calibrate the dynamic model with dedicated experimental data, and then apply it to simulate a variety of designed flash flood scenarios caused by cascading dam failures. Moreover, process-based flood dynamics and their evolution are explored in detail. Results indicate that cascading dam failures in a sloping channel cause an overall amplification of flash flood dynamics in the flow direction, but fluctuation of key hydraulic parameters occurs around each dam. Also, bigger landslide dams prevent upstream flood propagation better, but the blockage of the flows raises the potential flow energy. This implies a higher potential hazard risk in case of 'sudden-onset' failure of the dam. Moreover, the shape characteristic of a channel (straight or with bends) influences the evolution of the flash flood along the sloping channel. The findings enhance the understanding of the formation and evolution mechanisms of flash floods due to cascading failures of natural landslide dams, and hence are beneficial for assessing hazard risk and developing mitigation strategies for flash flooding in mountainous areas.

Keywords: landslide dam; cascading failure; flash flood; hydro-morphodynamic model

1. Introduction

Mountainous river valleys can be dammed when landslide or sediment movement reaches the river channel and results in complete or partial blockage of the valleys (Zhou et al., 2015; Liao et al., 2019). Intense rainfall and earthquakes have been considered as the main root causes to trigger the failure of natural landslide dams (Ermini and Casagli, 2003; Weidner et al., 2019). Different from conventional artificial dams, natural landslide dams typically comprise unconsolidated and poorly sorted materials and are vulnerable to failure following flow overtopping or dam seepage. Numerous pieces of field evidence have indicated that natural landslide dam failures have led to significant risk, e.g. the Wenchuan

* Correspondence to: Dr. Mingfu Guan, Assistant Professor, Department of Civil Engineering, University of Hong Kong, Email: mfguan@hku.hk

earthquake in 2008 resulted in 828 landslide dams and their failures induced severe flash floods (Fan et al., 2013; Shi et al., 2015). Studies have shown that over 90% of natural landslide dam failures are driven by flow overtopping and over 80% occurred within half a year of their formation (Schuster, 1986; Costa and Schuster, 1988). For many landslide dams in a river valley, intense rainfall induced streamflow can cause their failures, and the resultant flow evolves in a short period to be a large flash flood involving a high concentration of sediments (Iverson et al., 2011; Zhou et al., 2015). It is very likely for sediment-charged floods to be amplified along the flow direction due to the inclusion of a large amount of sediments. This can result in significant and sudden debris flow and cause severe damage to human lives and property downstream. For example, the 2010 Zhouqu debris flow in Gansu Province, China was triggered by intense rainfall upstream, and the sloping river gullies were blocked by a cluster of landslide dams and a number of constructed dams with much debris on the upslope of the dams (Dijkstra et al., 2012; Tang et al., 2011); thus, with the entrainment of sediment materials in the flow, the upstream flash flows enlarged along the sloping river gullies.

The failure mechanism of a single dam due to flow overtopping and subsequent hydraulics and morphological impact has been studied both experimentally (Coleman et al., 2002; Schmocker and Hager, 2010; Cao et al., 2011a; Chen et al., 2015; Jiang et al., 2018; Wang et al., 2018; Zhou et al., 2019) and numerically (Guan et al., 2014; Cao et al., 2011b; Di Cristo et al., 2018). Past research of a single natural dam failure mainly focused on the formation of a barrier lake upstream of the dam, and then the dam surface erosion due to flow overtopping, as well as the lateral dam erosion for partial dam failures (Wang et al., 2016). For single natural dam failure, a recent study by Bohorquez et al. (2019a) proposed a simple approach to reconstruct the failure model in natural dams to estimate the outflow hydrography due to dam breach. Chen et al. (2015) reported that dam geometry, inflow magnitude, hydraulic conductivity of dam material, and riverbed conditions have considerable effects on the lifespan of dams and their corresponding failure mode. Although there are studies in past decades focusing on the breaching process and flooding from artificial dams including cascading failures, the inherent differences between artificial and natural dams in terms of compaction and erodibility imply that existing findings from the artificial dam breaks cannot be directly used for natural dam breaks. The whole process of landslide dam failure is considered as a physical process of flow-energy conversion. The presence of natural dams in a valley can dramatically change downstream hydraulics, and the destructive power of the flow may be also increased. However, these studies have mainly focused on the breaching processes of an earthen dam and outflow discharge estimation, e.g. real-world barrier lake failure or river dyke breach (e.g. Walder and O'Connor, 1997; Coleman et al., 2002; Guan et al., 2014; Di Cristo et al., 2018). In mountainous valleys, it is common for landslides to form a series of sediment blockages (or dams) (Ermini and Casagli, 2003). As stated, previous studies have mostly concentrated on the failure mechanism of a single dam due to gradual flow overtopping. However, flash flood evolution in a sloping channel with a cluster of natural landslide dams is a much more complex process, i.e. one dam failure directly affects the failure process of downstream dams. It is recognized that sediment materials from riverbeds and banks play an important role in the growth of downstream debris flow and flash flooding in terms of both size and speed (Berger et al., 2010;

Iverson et al., 2011; Cui et al., 2013). It is therefore desirable to investigate the detailed hydraulic processes of cascading failures of a cluster of natural dams that provide abundant sediment materials for entrainment.

Field investigations have been conducted to explore the fundamental failure mechanisms of a cluster of landslide dams (e.g. Zhou et al., 2015; Cui et al., 2013) and engineering mitigation measures (e.g. Peng et al., 2014). For example, Cui et al. (2013) investigated post-flood field sites after a flash flood caused by dam failures. The study estimated the peak water level based on the fresh sediment marks in a valley and quantified the erosion and sedimentation based on pre- and post-flood bed elevations. However, the sudden, unexpected nature of landslide dam failures makes it nearly impossible to foresee where and when the failure will happen. This leads to the difficulty in monitoring the full failure process of dams; thus, the resultant understanding may not be comprehensive. Laboratory-scale experiments, built on field cases, have also been carried out for cascading dam failures, including three groups of situations: due to clear water in a steep slope channel, in a flat erodible channel, and in a steep erodible channel. First, Xue et al. (2011) adopted sluice gates to reproduce clear-water flow that induces a cascading dam failure in a steep slope channel. The dam-break process is achieved by suddenly lifting the gate that holds the water, which is rarely seen in reality. Second, experiments of a cascading dam failure in a flat and erodible channel (Cao et al., 2011a; Shi et al., 2015) showed that the presence of the second dam delays the flood arrival time and increases the depth and peak discharge downstream. However, the channel slope considered was small and multiple dam failures have not been well investigated, so the findings cannot well represent the hydrodynamics of flash flooding in a sloping mountainous valley with a cluster of sediment blockages. To mimic sediment-charge flows in mountainous steep channels, Iverson et al. (2011) conducted entrainment experiments by undertaking a one-off flash flow over a steep erodible flume and revealed how static sediment can result in conspicuous flow-momentum growth. But the flow behaviors differ from those with a cluster of natural dam blockages. Some studies (e.g. Niu et al., 2012; Chen et al., 2014; Zhou et al., 2015) have exploited debris and gravel to mimic the fully blocked and partial blocked landslide natural dams in a steep erodible channel where the flow propagates and evolves into a large debris flow. For these experiments, the channel slope varied from 5% to 30%. High-speed cameras were applied to video the debris front, and laser depth sensors were used to record the temporal variation of flow depth at certain positions. Such observed data and information support better understanding of the mechanism and evolution of flash floods due to a cascading failure of natural landslide dams. However, the restrictions of experiments in temporal and spatial monitoring limit the reproduction of full dynamic processes. The mechanism of mass and flow growth due to a series of natural dam failures in a steep valley has remained unclear. The lack of data obtained under controlled conditions has been considered to be partly responsible (Iverson et al., 2011). Recent developments in reliable numerical models have helped to develop a greater understanding of hydraulics for the evolution of sediment-laden flows. A well-validated and calibrated full dynamic numerical model is able to fill this gap with more detailed hydraulics information.

This study therefore seeks to address the aforementioned research gaps by establishing a numerical model to mimic flash flood evolution with the failure of a cluster of landslide dams in a steep channel that may occur in nature. The study systematically evaluates the effects of dam blockages with varying numbers and sizes, and the influence of the channel shape feature on downstream flood evolution. Detailed flood hydrodynamics and the mechanism of flow growth are examined at a high spatio-temporal scale. First, the study exploits the experimental data by Chen et al. (2015) to calibrate a hydro-morphodynamic model that is a coupled 2D shallow water model and bedload dominant sheet flow model (Guan et al., 2014; 2015; 2016); then, the dynamic model is further applied to 8 designed natural dam failure scenarios, including a variety of dam numbers and sizes, as well as straight and bend channels. To our knowledge, such a systematic study based on detailed numerical modeling has not been undertaken before. The results provide evidence-based understanding of the formation, evolution, and mechanism of flash flooding in mountainous valleys.

2. Computational Model

2.1. Hydro-morphodynamic model

The hydro-morphodynamic model is governed by 2D shallow water equations and a non-equilibrium sediment transport model that have been intensively developed (e.g. Cao et al., 2004; Wu and Wang, 2007; Guan et al., 2014). In mountainous areas, bedload is generally the dominant transport mode; therefore, the sheet flow model dominated by bedload and partially suspended load is used in this study. More details about the model and numerical algorithm are described in Guan et al. (2014). Governing equations are expressed by

$$\frac{\partial \eta}{\partial t}+\frac{\partial hu}{\partial x}+\frac{\partial hv}{\partial y}=0 \tag{1}$$

$$\frac{\partial hu}{\partial t}+\frac{\partial}{\partial x}\left(hu^2+\frac{1}{2}gh^2\right)+\frac{\partial}{\partial y}huv=gh\left(S_{ox}-S_{fx}\right)+\frac{\Delta\rho u}{\rho}\frac{\partial z_b}{\partial t}\left(\frac{1-p}{\beta}-C\right)-\frac{\Delta\rho gh^2}{2\rho}\frac{\partial C}{\partial x} \tag{2a}$$

$$\frac{\partial hu}{\partial t}+\frac{\partial}{\partial x}huv+\frac{\partial}{\partial y}\left(hv^2+\frac{1}{2}gh^2\right)=gh\left(S_{oy}-S_{fy}\right)+\frac{\Delta\rho v}{\rho}\frac{\partial z_b}{\partial t}\left(\frac{1-p}{\beta}-C\right)-\frac{\Delta\rho gh^2}{2\rho}\frac{\partial C}{\partial y} \tag{2b}$$

$$\frac{\partial hC}{\partial t}+\frac{\partial huC}{\beta\partial x}+\frac{\partial hvC}{\beta\partial y}=-\frac{(q_b-q_{b*})}{\beta L} \tag{3}$$

where h = flow depth (m); z_b = bed elevation (m); $\eta = h + z_b$ denotes the water surface elevation, which includes both changes in the water depth and bed elevation varying with time t (s); u and v = the depth-averaged flow velocity components in the two Cartesian directions (m/s); g = acceleration due to gravity (m/s^2); p = sediment porosity (dimensionless); C = volumetric sediment concentration (dimensionless); $\Delta\rho = \rho - \rho_w$ = the difference in sediment density (ρ_s) and water density (ρ_w) (m^3/s); $\rho_m = \rho_w(1-C)+\rho_s C$ = density of flow-sediment mixture (m^3/s); S_{ox}, S_{oy} are the bed slopes in the x and y direction expressed by $S_{ox} = -\frac{\partial z_b}{\partial x}$, $S_{oy} = -\frac{\partial z_b}{\partial y}$; S_{fx}, S_{fy} are the frictional slopes in the x and y direction calculated based on Manning's roughness n (m$^{-1/3}$s) by $S_{fx} = \frac{n^2 u\sqrt{u^2+v^2}}{h^{4/3}}$; $S_{fy} = \frac{n^2 v\sqrt{u^2+v^2}}{h^{4/3}}$; and L = non-equilibrium adaptation coefficient of sediment transport (m) determined by Guan et al. (2014):

$$L = \frac{h\sqrt{u^2+v^2}}{\gamma\omega} \text{ with } \gamma = \min\left(\beta\frac{h}{h_b}, \frac{1-p}{C}\right) \quad (4)$$

in which, p is sediment porosity, $h_b = 9\vartheta d_{50}$ is the thickness of sheet flow layer estimated according to Pugh and Wilson (1999) and Ferreira et al. (2009), and ϑ is the dimensionless bed shear stress. Flow-to-sediment velocity ratio β is calculated by

$$\beta = \begin{cases} \dfrac{u}{u_b} = \dfrac{u}{u_*}\dfrac{\sqrt{\theta_c}}{1.1(\theta/\theta_c)^{0.17}[1-\exp(-5\theta/\theta_c)]} & \theta/\theta_c < 20 \\ 1 & \theta/\theta_c \geq 20 \end{cases} \quad (5)$$

where $u_* = \sqrt{\theta(\rho_s/\rho_w - 1)gd}$ is the shear velocity; d is the median sediment diameter; and θ_c is the critical dimensionless bed shear stress for sediment motion incipient calculated by the formula proposed by Soulsby (1997). The Meyer-Peter and Müller equation (*MPM*) has been recalibrated by Wong and Parker (2006), and the below updated formula is used to calculate the bedload-dominant transport rate:

$$q_{b*} = 4.93(\theta - 0.047)^{1.6}\sqrt{(\rho_s/\rho_w - 1)gd^3} \quad . \quad (6)$$

The morphological evolution is determined by the difference between the real sediment transport rate and the sediment transport capacity, which is calculated per grid cell at each time step:

$$\frac{\partial z_b}{\partial t} = \frac{1}{1-p}\frac{(q_b - q_{b*})}{L} \quad (7)$$

where $q_b = hC\sqrt{u^2+v^2}$ is the actual sediment transport rate.

Equations (1) to (3) constitute a shallow water non-linear system and they are numerically solved by a well-balanced Godunov-type shock capturing numerical algorithm based on Cartesian coordinates, described in detail in Guan et al. (2014). A variable time step, adapted to hydraulic parameters variability, is calculated based on the Courant number. As the numerical scheme is explicit, the Courant number is restricted to 0<CFL<1.0 for the solution of the coupled model. The numerical model has been validated by a series of laboratory experiments (Guan et al., 2014). This includes dam-break flow over an erodible bed with fixed width and sudden enlarged width, dam erosion due to flow overtopping, and earthen dyke breach due to flow overtopping. The validations verify that the model is capable of reasonably reproducing the full hydro-morphodynamic processes of natural dam/dyke/embankment erosion, including hydrodynamics and bed change simulations. The mathematical model aforementioned is applied below for simulating flash flooding due to a cascade of landslide dam failures.

2.2. Scenarios for numerical investigation

Experiments have been conducted by Chen et al. (2014) to reproduce a cascading failure of natural landslide dams. The experiment demonstrates the formation and evolution of a flash flood with inclusion of a high concentration of sediments. Although hydraulic data was measured, and understanding of the flash flood dynamics was developed, the limitations of the experimental conditions and measurement capability led to a lack of detailed dynamic data for comprehensive hydraulic analysis. Therefore, numerical investigations are conducted based on this experiment and wider designed scenarios that may

occur in the real world. The baseline model scenario (Case 3 in Table 1) is the failure of a cluster of partial dams (3 dams) observed in Chen et al. (2014). Therein, the experimental flume is composed of an upstream water tank with a horizontal bottom of 4.6 m long, 0.7 m wide and 1.4 m high, and a downstream channel with a steep slope of 12° and that is 47.3 m long, 0.7 m wide and 1.4 m high (Figure 1). The initial water volume in the water tank is 1.45 m^3 and water depth is 0.45 m. A sluice gate was used to control the water depth of the upstream water tank. The gate is suddenly lifted to induce a first dam-break flash flood. Then, the floodwater flows over a series of partial blocked natural dams that are set in the downstream of the channel at regular intervals. Each dam is defined as a semi-spheroid with long axis (a), short axis (b) and height (h). The sediment obtained in the field is a mixture of sand and clay, and the particle parameter is estimated to be 0.015 m. According to in-situ measurement, the density of sediment is 2650 kg/m^3, the dry density of the sediment mixture is 1830 kg/m^3, and the bed sediment porosity is about 0.6. For other scenarios, channel conditions and sediment materials are the same, but the numbers of natural dams and their size are set differently in order to examine the effects of channel blockage percentage on flash flood hydraulics. Designed scenarios are described in Table 1 and illustrated in Figure 1. Time series of water depth at points C1 and C3 are measured for the baseline Case 3, and they are used to calibrate the dynamic model. To analyze the impact of sediment transport, a scenario without sediments in the channel (Case NS) and a scenario with a flat layer of sediment (Case 0) are also simulated.

Studies have indicated that it is common to have mountainous rivers or valleys shaped in a bend that may remarkably alter the propagation and evolution of flash floods (Miller and Chaudhry, 1989; Bai et al., 2007; Zhou et al., 2012). Nonetheless, the bend effect on a cascading failure of natural dams has not been discussed and remains unclear. Thus, we also come up with simulation scenarios of landslide dam failure in a bend channel. The setup of dams is kept the same as that of a straight channel, except that the channel has been changed into a 90-degree bend with a radius of 26 m, and the longitude coordinate is shifted to the arc length. The origin point of the arc length is set at the center of the sluice gate. For simplicity, only case 4-1 with a bend channel is shown in Figure 2.

The simulation region covers the water tank and the 47.3m long and 0.7m wide flume, which is discretized by 0.025×0.025 m^2 meshes. The major parameters for the modeling scenarios are listed in Table 2, and the roughness coefficient is calibrated in a range of 0.015–0.04.

Table 1. Modeling scenarios for straight and bend channels

Scenarios	Sediments layout	Dam shape and size
Case NS	No sediments in the channel	
Case 0	No dam in the channel, but 5 cm thick sediments are set from gate to x (or arc length) =20.65m	
Case 1	1 dam and 5 cm thick sediments are set from gate to x (or arc length) =20.65 m	Semi-spheroid, a=1.45,b=0.7,h=0.5
Case 2	2 dams and 5 cm thick sediments are set from gate to x (or arc length) =20.65 m, 27.15 m	Same size a=1.45,b=0.7,h=0.5
Case 3	3 dams and 5 cm thick sediments are set from gate to x (or arc length) =20.65 m, 27.15 m, 33.65 m	Same size a=1.45,b=0.7,h=0.5

Case 4-1	4 dams and 5 cm thick sediments are set from gate to x (or arc length) =20.65 m, 27.15 m, 33.65 m, 40.15 m	Same size a=1.45,b=0.7,h=0.5
Case 4-2	4 dams and 5 cm thick sediments are set from gate to x (or arc length) =20.65 m, 27.15 m, 33.65 m, 40.15 m	Dam4 a=1.45,b=0.7,h=1.0
Case 4-3	4 dams and 5 cm thick sediments are set from gate to x (or arc length) =20.65 m, 27.15 m, 33.65 m, 40.15 m	Dam4 a=1.45,b=1.0,h=1.0

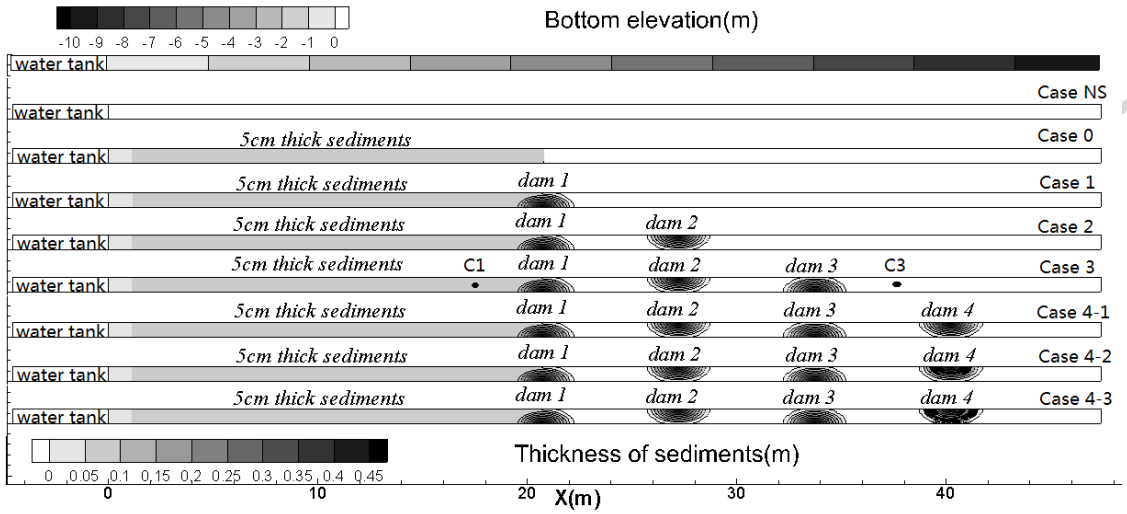

Figure 1. Modeling scenarios for a straight channel

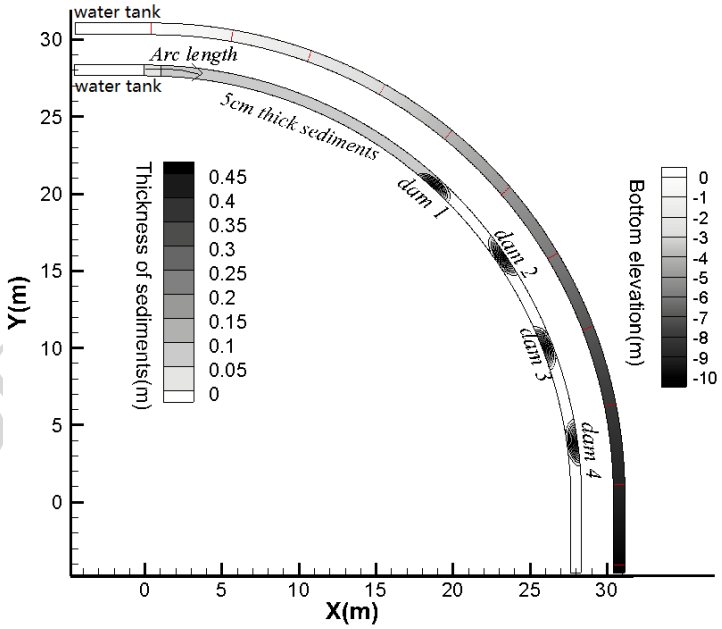

Figure 2. Modeling scenarios for a bend channel (case 4-1)

Table 2. Parameters for the modeling scenarios

Model parameters	$\rho_s(kg/m^3)$	$\rho_w(kg/m^3)$	p	d(m)	mesh size (m×m)
Value	2650	1000	0.6	0.015	0.025×0.025

3. Results

3.1. Model validation and calibration

Shallow water-based models have been considered as an effective approach in simulating hydraulics and morphological changes induced by shock-capturing flows (Bohorquez et al., 2019b). The model applied in this study has been well validated by a series of laboratory experiments (Guan et al., 2014). Validation studies have shown that the model is capable of simulating single dam erosion due to flow overtopping, and partial breach of a single dyke. It has been demonstrated that water depths, dam profile changes, and time series of outflow discharge can be well simulated by the shallow water-based numerical model. This provides the basis of the model application in the failure of a cluster of natural dams.

Manning's roughness has been indicated as the key parameter in the model to calculate bed shear stress and sediment transport rate, which will affect simulation results. Therefore, Manning's roughness is calibrated by comparing simulated and measured time series of water depth at the two gauges, C1 and C3, for the baseline scenario (Case 3). Figure 3 plots the measured data and simulated results with different Manning's roughness values (n=0.015, 0.02, 0.025, 0.03, 0.035, 0.04 $sm^{-1/3}$). It shows that the magnitude and trend of water depth at both C1 and C3 are reasonably simulated. At both points, the water depth rises sharply once flash waterfronts arrive, and a recession follows the peak value. The flash period lasts about 5 seconds, and it is followed by a gentle decreasing stage. C1, located in the erodible bed with a thickness of 5 cm, is eroded by the flash flow. As Manning's roughness affects both flow velocity and sediment transport rate, we can see that the waterfront reaching times with different Manning's roughness values differ at both C1 and C3, particularly at the downstream gauge C3. It is clear that the higher value leads to a slow waterfront speed, thereby causing a longer time to reach the point. By comparing the six simulated curves with measured data and also analyzing the NSE (Nash-Sutcliffe Efficiency) coefficient and RMSE (Root Mean Square Error) in Table 3, we take Manning's roughness as n=0.025 for the modeling of other scenarios. Morphological change in Figure 4 shows that the erosion of the dams along the channel is also simulated reasonably well. As above, the simulated results, while as expected not perfect, are deemed as satisfactory for reproducing the flash flood dynamic process. The discrepancy between simulated and measured results mainly stems from the following reasons. (1) The flash flow occurs rapidly within a few seconds, and the flow depth is small, so the laser equipment must create errors in the measured data. For example, the majority of the measured data at C1 after 10 s is slightly smaller than zero. (2) Random lateral collapse occurs during each dam failure in experiments, but it is difficult to capture the processes. (3) Non-uniform sediment materials are used, but we adopted a median representative diameter in the model. Also, empirical formulae may bring in simulation errors. As shown in Figure 3, the discrepancy mainly occurs in the recession stage (e.g. around 10s at C1), because the depth in this stage is small, the numerical model has an inherent error when modeling sediment transport in relatively shallower flows, and the laser equipment can lead to extra errors in measuring the flow depth. Despite this discrepancy, the model is verified to be able to reproduce the dynamic process of the cascade failure of a series of natural dams as shown in Figure 3.

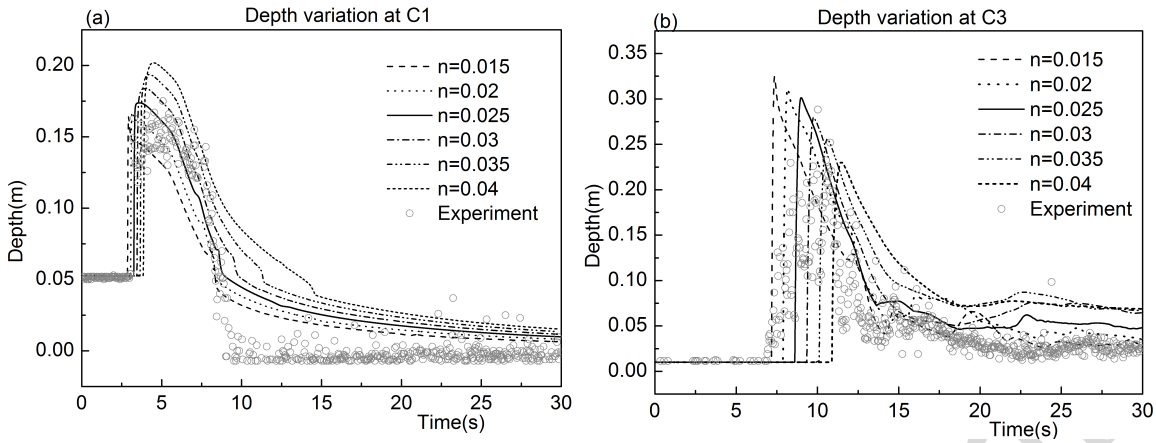

Figure 3. Simulation and experiment results of case 3 under different roughness values

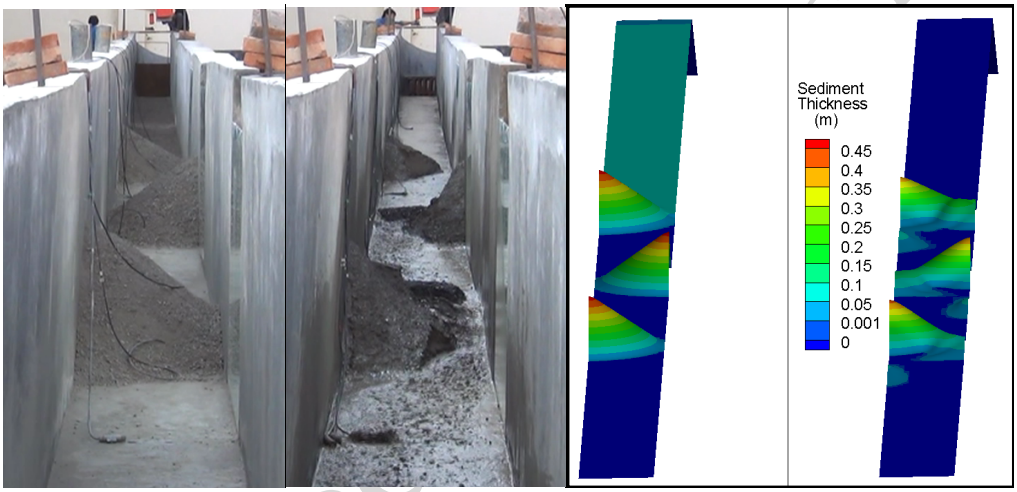

Figure 4. Bed form before and after the flood for the experiment and numerical simulation

Table 3. NSE and RMSE under different roughness values at C1 and C3

	n($sm^{-1/3}$)	0.015	0.02	0.025	0.03	0.035	0.04
C1	NSE	0.831	0.834	0.867	0.759	0.651	0.489
	RMSE(m)	0.023	0.023	0.020	0.027	0.033	0.040
C3	NSE	0.454	0.468	0.507	0.395	0.112	-0.209
	RMSE(m)	0.039	0.038	0.037	0.041	0.050	0.058

3.2. Flash flood evolution over a cascade of dams

Still for the baseline Case 3, Figure 5 illustrates bed elevation and surface water level averaged over each cross section around the three natural dams. It clearly shows that the flash waterfront reaches the top of dam 1 at about 5 seconds, propagates to the front of dam 2 at about 6 seconds, and passes over dam 3 at 8 seconds. The flash flood induces a considerable amount of sediment to be transported with the flow, leading to severe erosion of each dam (final bed elevation curve in Figure 5), and the dam erosion is more severe in the upstream section of the channel. For example, dam 1 and the upstream channel bed are severely eroded, while sediment material deposits at the upslope region of dam 3. This is attributed

to the blockage effects of downstream dams, which trap an amount of sediments. Similar behavior has also been observed in the laboratory experiment presented by Chen et al. (2014). This physical process of the formation and evolution of flash floods involves both sediment erosion and the collapse of an amount of sediments that are subsequently transported by the flashing flow. This is also consistent with real-life field observations (e.g. Walder and O'Connor, 1997). To develop further understanding of the physical processes, Figure 6 plots the simulated peak flow depth along the channel over the whole flood period and field depth. Field depth is quantified as the difference between peak water level and final bed elevation, and it is generally used in the field to estimate flow discharge after a real-world flood event (Sayama et al., 2019). Figure 6 indicates that peak depth is overall smaller than field depth along most of the channel, except upfront toe and the area downstream of dam 2 and dam 3. The difference between peak depth and field depth is particularly remarkable in regions where severe erosion and deposition occur, while it is quite insignificant in areas without much change in the bed. This implies that discharge estimations from using the traditional approach of field depth may differ greatly from real values. This indicates the advantages of and need for a dynamic model to improve understanding of cascading failures of a cluster of natural dams.

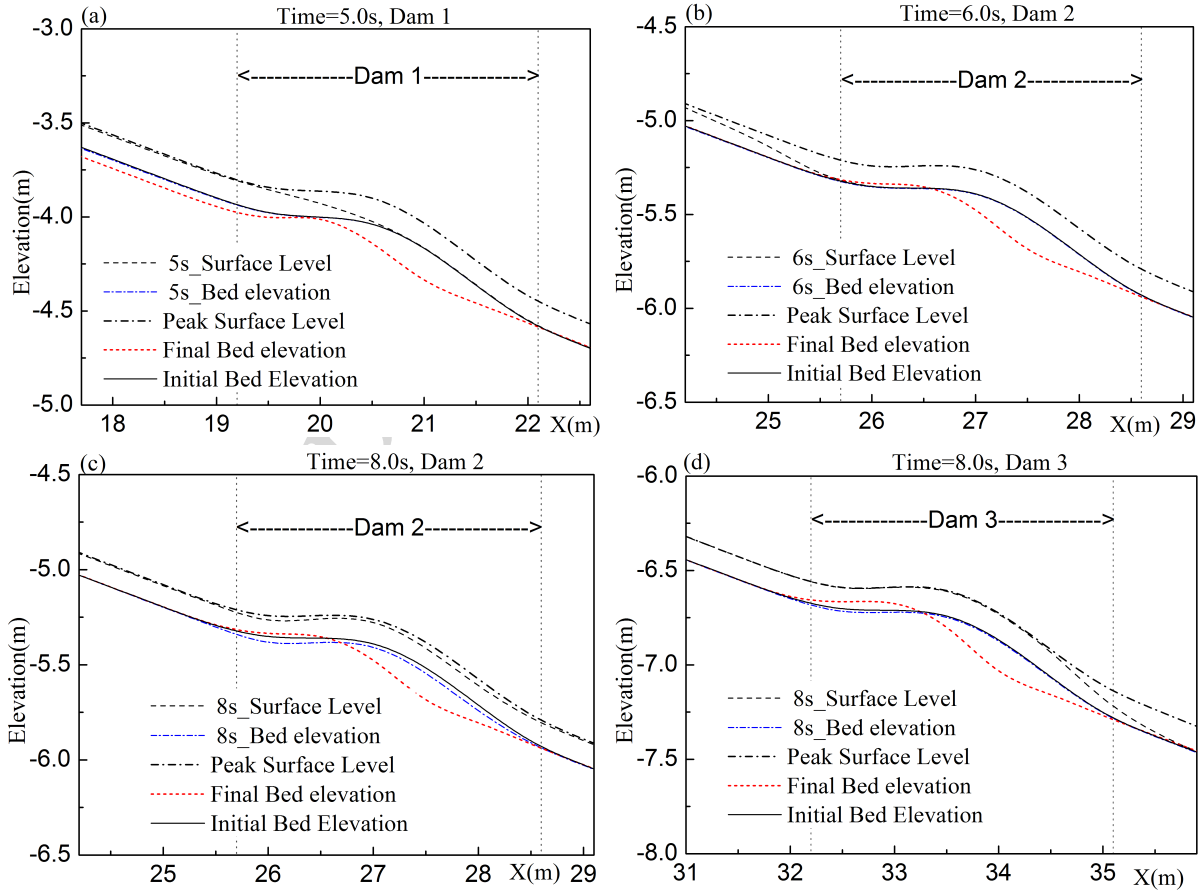

Figure 5. Surface level and bed elevation near the dams; note, vertical dash line denotes the start and end point of each dam

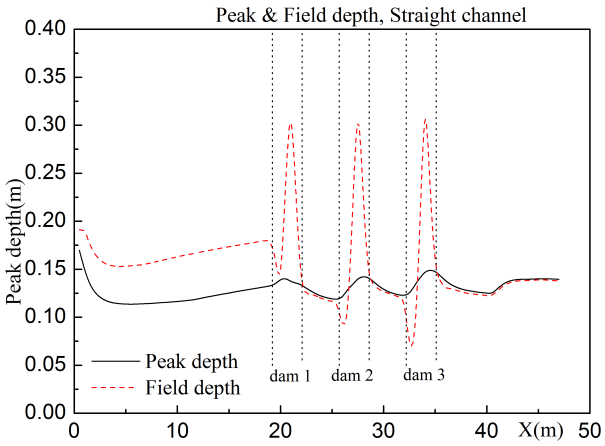

Figure 6. Peak depth and field depth along the channel

A number of studies have reported that outburst floods can induce a considerable amount of sediment transport, and the bulk effects of sediment entrainment will raise the volume and peak discharge of the flow (Guan et al., 2015; Cui et al, 2013). This feature has also been verified in current numerical investigation. Figure 7 demonstrates the flow depth and unit flow discharge in front of and at the end of dam 3. It clearly shows that both peak flow depth and peak discharge over the flood period are increased by about 17% and 11%, respectively. Overall, simulated results of the experimental baseline case show that natural dams in a valley play an important role in preventing flash flood propagation; however, in case of their failure, the flash flood magnitude may be remarkably increased in terms of both depth and discharge. The amplification effects due to the involvement of sediments in floods is considered as a key indicator for flash flood risk management in mountainous areas.

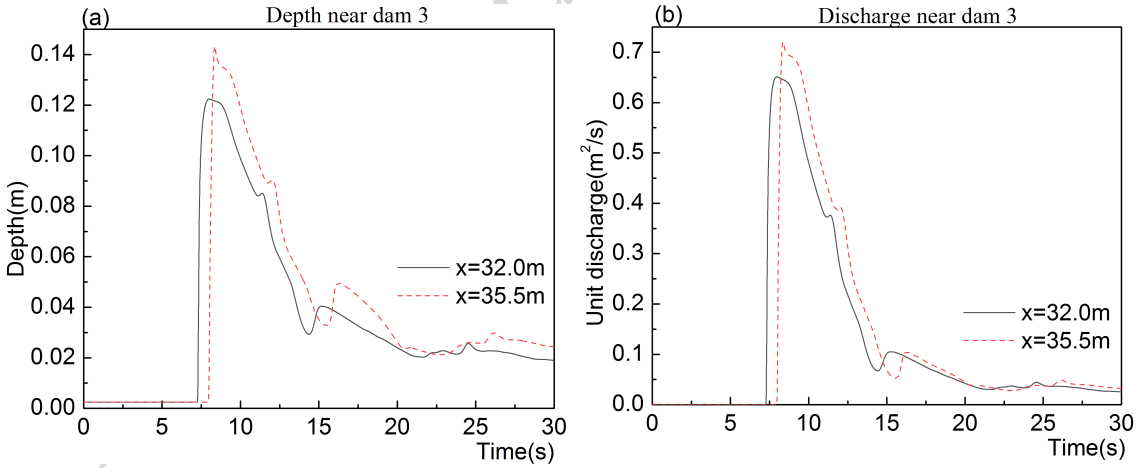

Figure 7. Time series of flow depth and unit discharge in front of and at the end of dam 3

3.3. Failure of a cascade of natural dams in a straight channel

As listed in Table 1, this study examines 8 scenarios, including a no-dam fixed channel, an erodible channel without dams, and erodible channels with 1, 2, 3 and 4 dams. This allows us to explore the formation and evolution of sediment-charged flash floods in a steep channel and how natural dams affect

hydrodynamics. As peak water depth, peak velocity, peak discharge, and peak energy are generally considered as the most important indicators for risk assessment, we exploit the model to track peak values of these variables along the channel (Figure 8). Therein, the energy is defined as

$$E = z_b + \left(\frac{u^2 + v^2}{2g} + h\right)\rho_m/\rho_w \,. \tag{8}$$

Results show that, for Case NS, peak flow depth decreases at the starting reach of the channel and approaches to a constant in the downstream region. Correspondingly, peak velocity first increases once a sluice gate is lifted, and then reaches a nearly constant value downstream. However, sediment entrainment from the channel bed increases the peak flow depth. Although the velocity is reduced before the waterfront reaches the endpoint of the erodible bed (e.g. curves for Case 0), the value remarkably increases in the downstream region, and it is larger than that for Case NS. Also, it is seen that the presence of natural dams in the channel leads to an increase of peak depth, peak velocity, and peak discharge (Figure 8 a-c). A dam first increases the flow depth in front of it, and then the peak depth reduces after the flow passes over it. Figure 8(b) indicates that at first sediment erosion adds extra resistance to the flow acceleration, which contributes to a slower increase in velocity. Nevertheless, the flow keeps absorbing the sediment, and the flow volume due to sediment entrainment expands, which makes the velocity become even larger. In each dam region, peak velocity falls at the upstream side of the dam as the elevation goes up, while it rises at the downstream side due to the acceleration of gravity. Regarding flow discharge, Figure 8(c) also shows an overall rising trend in spite of a fluctuation around each dam. By comparing the curves from Case 1 with Case 4, where the number of dams increases from 1 to 4, we can conclude that each increase in the number of dams in the channel will bring peak depth, velocity, and discharge one step higher in case of failure of the dam. The effects of sediments in the channel on hydrodynamics are reflected in energy conversion along the channel. The peak energy profile in Figure 8(d) shows that there is the smallest peak energy amongst all cases for the clear-water no-dam scenario (Case NS), $\rho_m/\rho_w = 1.0$, and the peak energy decreases linearly in the flat bed part. When the flow reaches the natural dam region, the peak energy decreases in the downstream side of the dam and recovers in the region between dams. The region where peak energy falls the most is also the high peak velocities area, where bed resistance dissolves more energy.

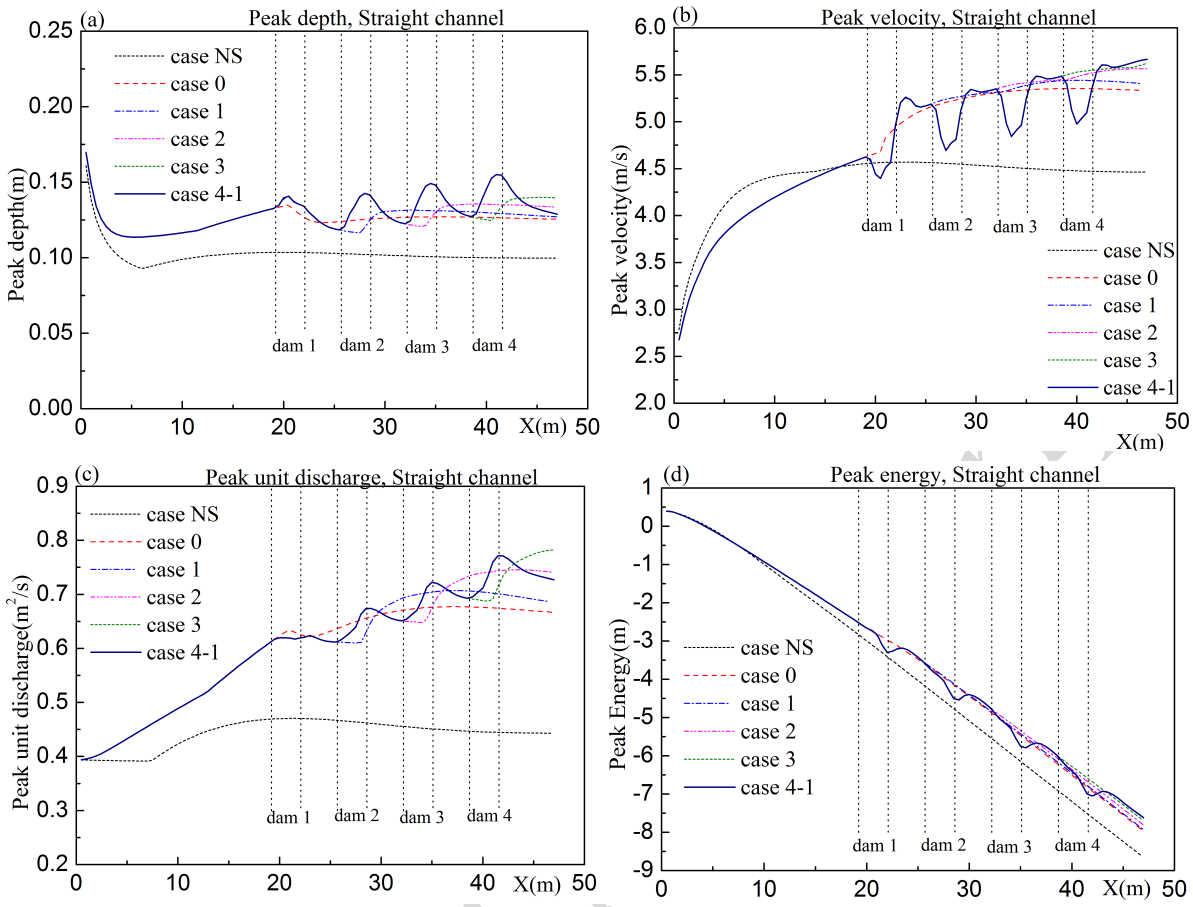

Figure 8. Simulated peak depth, velocity, unit discharge, and energy along the straight channel

The results above demonstrate how a series of natural dams affect flash flood hydrodynamics in a sloping channel. In reality, landslides can cause a number of natural dams of multiple types to develop and be distributed closely together in a valley (Korup et al., 2010; Cui et al., 2009). Their sizes and shapes can differ. Therefore, this study also examines the effects of natural dams on the evolution of flash floods. For four-dam scenarios, we further simulate the full dynamic process for dam 4 with different sizes. In case 4-1, the 4 dams have the same size, while in case 4-2 and case 4-3, dam 4 is double and triple the size, respectively, of the 3 upstream dams. Figure 9(a) shows that a bigger dam blocks more water, and hence there is a higher peak depth at the dam upstream. This implies that the peak velocity at the upstream of dam 4 is also reduced due to the blockage effects; however, the peak velocity at the downslope of dam 4 is raised. Although peak flow discharge overall increases along with the channel (Figure 9c), the bigger-sized dam 4 plays a key role in slowing down the evolution and amplification of the flash flood. Moreover, the peak energy profile in Figure 9(d) clearly indicates that the total flow energy after passing over the bigger-sized dam 4 is raised, which suggests that the flash flood will have greater potential to cause downstream destruction.

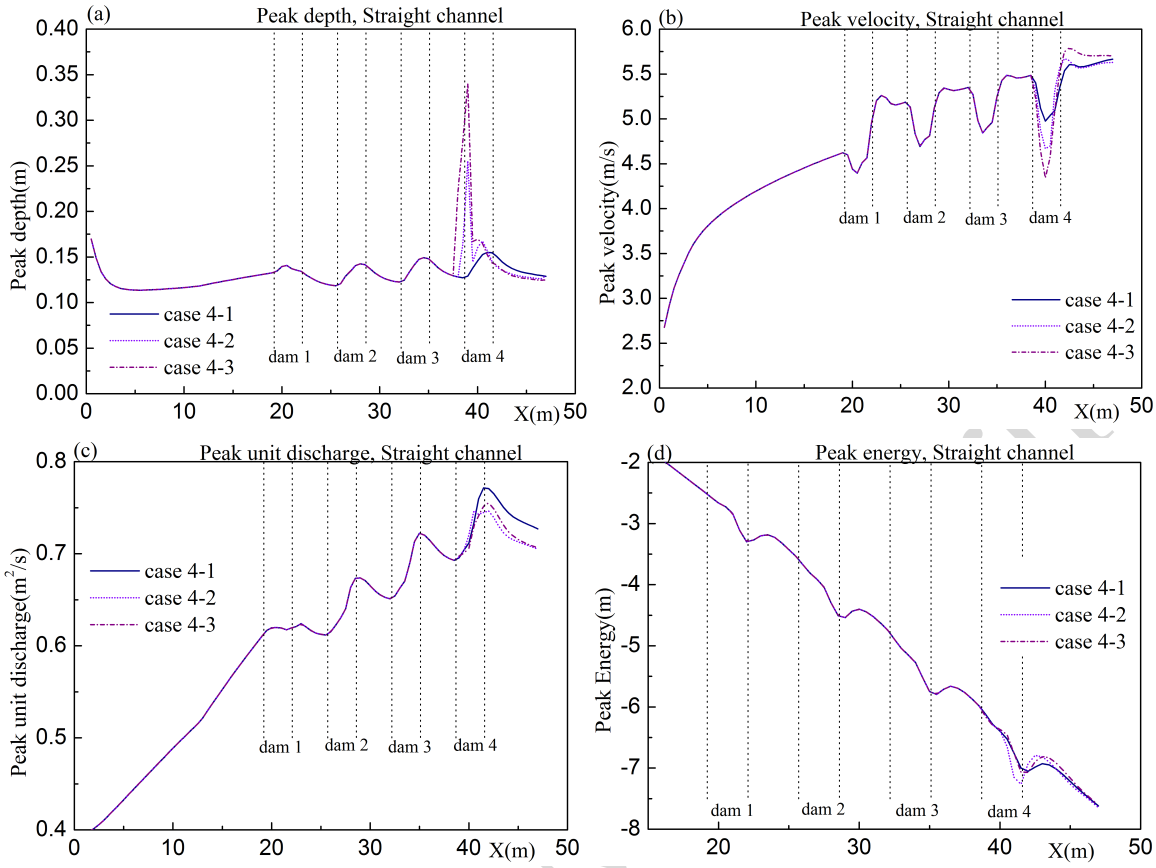

Figure 9. Simulated parameters along the straight channel (different dam sizes)

3.4.Cascading failure of a landslide dam in a bend channel

For the bend channel scenarios, dam 1 and 3 are located on the convex side of the bend, and dam 2 and 4 are on the concave side. Overall, the flash flood evolves in the bend channel with similar features as in the straight channel, i.e. the magnitude of the flash flood is amplified with more natural dams in the channel, and the increase is reflected in terms of peak depth, peak velocity, and peak discharge. However, it is seen that the amplification effect on flow discharge in dam 2 and 4 (concave side) is more significant than that in dam 1 and 3 (convex side). Regarding the propagation of the flood wave, Figure 10(b) indicates that the wave flows over dam 1 and a failure occurs, then a stronger wave (high speed) will form and move downwards, crushing the other dams downstream and causing more severe failure. Similarly, the bigger-sized dam 4 can prevent more flow passing through and slow down the erosion processes. Figure 11(a) shows that the peak depths in the dam regions are nearly the same for both the straight channel and bend channel; however, in regions downstream of the convex-side dams (dam 1 and 3), peak depth in the bend channel is smaller than that in the straight channel, and in regions downstream of concave-side dams (dam 2 and 4), peak depth in the bend channel is larger than that in the straight channel. The convex-side dams result in the weaker effects on the downstream depth, because of the flow characteristics of higher velocity at the outer side of a bend, which allows the flow to propagate more easily through the opposite side of dam 1 and 3. The presence of dam 1 and 3 is actually equivalent to narrowing the channel, and thereby a higher velocity is found around the dams in the convex side. In contrast, the flow discharge,

quantified based on depth and velocity, is particularly increased after the flow passes over concave-side dams (dam 2 and 4).

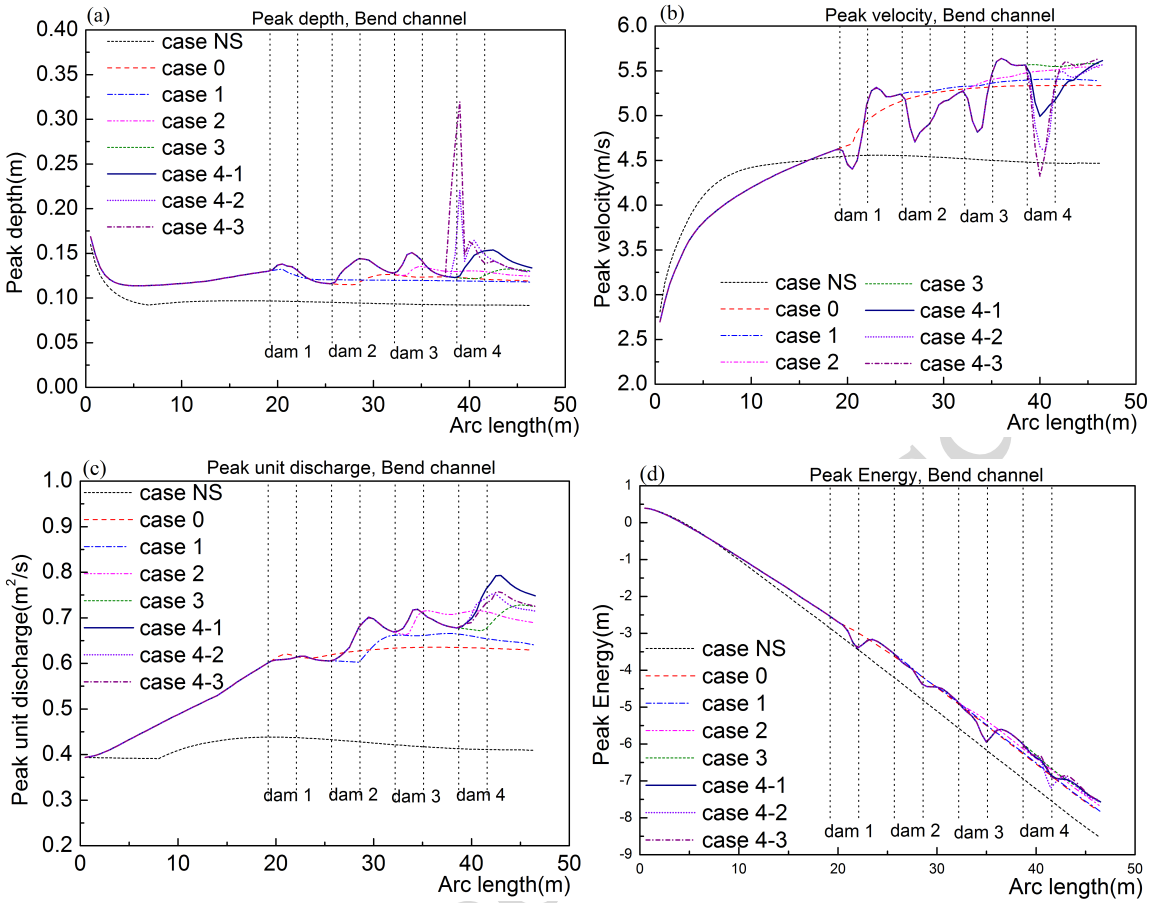

Figure 10. Simulated peak depth, velocity, unit discharge, and energy along the bend channel

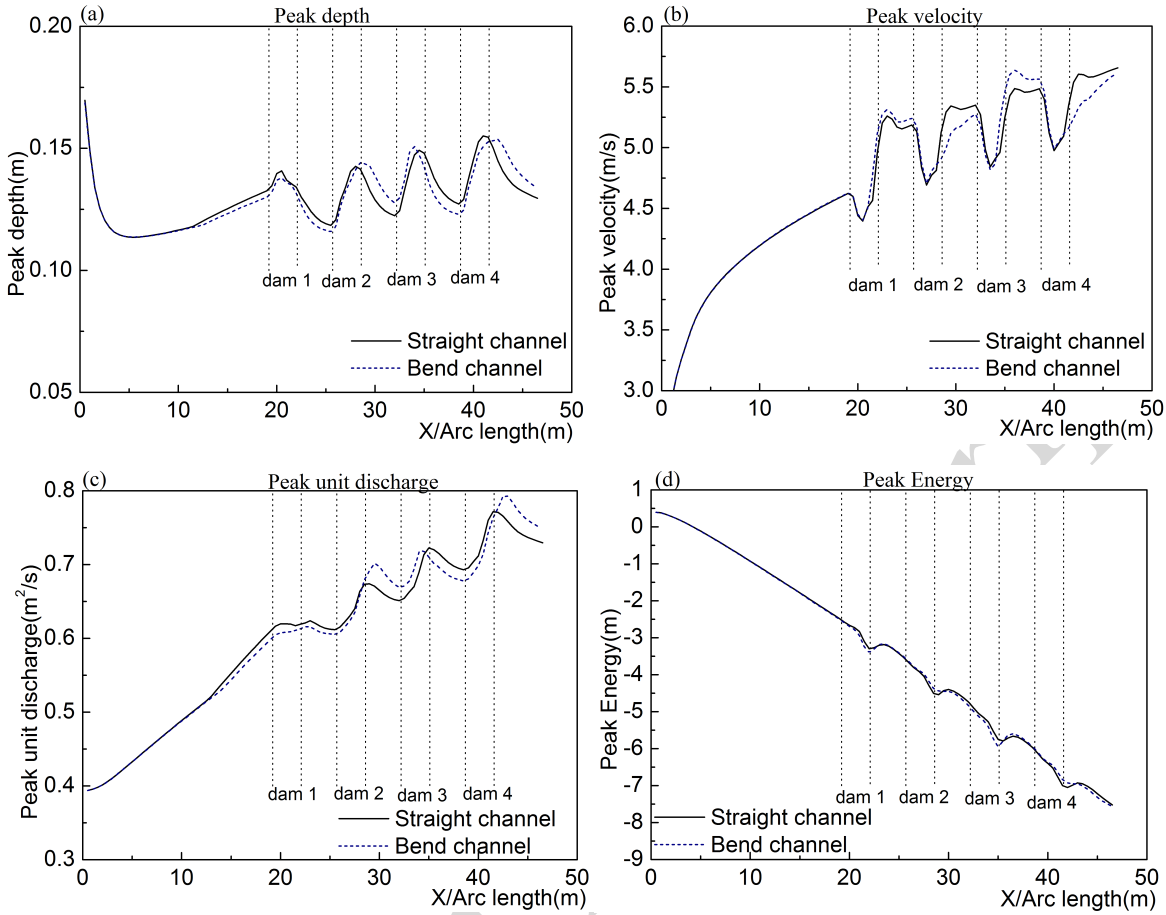

Figure 11. Comparisons between the straight channel and bend channel (case 4-1)

4. Discussion

4.1.The dam failure mechanism that field and lab investigations cannot observe

Landslide dam failure is an interdisciplinary topic that is related to geotechnics, soil mechanics, sediment dynamics, and river hydraulics. There are a number of interrelated physical parameters that are not yet determined. This may limit the results of mathematical modeling, which also makes assumptions. However, for both field and laboratory investigations, the lack of robustness of scenario designs, as well as the scarcity and unreliability of monitoring data, will limit the detailed understanding of full dynamics due to a cascading failure of landslide dams. This study therefore combines field and experimental studies with mathematical modeling to reproduce the full dynamics of landslide dam failures under a variety of scenarios, and detailed landslide hydraulics are reasonably quantified.

It has been reported that for a single landslide dam (e.g. barrier lake), dam erosion and breach occurs due to flow overtopping at an early stage, and then sediments from the lateral collapse of the dam are entrained and transported by the flowing water (Costa and Schuster, 1988; Coleman et al., 2002; Morris et al., 2007; Wang et al., 2016). Efficient models are generally studied to estimate outflow discharge due to dam breach (e.g. Walder and O'Connor, 1997; Cao et al., 2011b; Guan et al., 2014; Bohorquez et al., 2019a). However, results in this study show that downstream hydraulics are remarkably affected by dam

failures upstream; hence, some models for estimating outflow discharge cannot be simply extended for discharge estimation caused by a cascading failure of several landslide dams, e.g. reconstruction methods that are built on the post-flood water mark and final bed. The results in Figure 6 indicate that discharge estimations calculated through the traditional field depth approach (using the difference between the flood mark and final bed) may vary greatly from real-world values. A dynamic model is therefore needed to improve understanding of the cascading failure of a series of natural dams. Regarding the effects of riverbed mobility on flow arrival time, experimental results in Chen et al. (2015) found that a movable riverbed delays the arrival time of peak sediment discharge more significantly than a rigid riverbed; yet, this is not always true. A number of numerical and field studies on real-world events (e.g. Staines and Carrivick, 2015; Guan et al., 2016) emphasized that sediment entrainment may smoothen the channel, thus accelerating the flood propagation. Figure 7(b) shows that sediment entrainment indeed slows down the peak flow velocity at the initial channel breach in comparison with the flow over the rigid bed, but the peak velocity increases downstream.

4.2.*Physical differences between a single and cascading dam failure*

A natural landslide dam is formed of an unconsolidated mixture of earth-surface mass or debris in a naturally unstable state, and it is therefore vulnerable to entrainment by flash flooding (Iverson et al., 2011; Iverson and Ouyang, 2014). Results in Figure 6 show that an upstream flash flood induces a considerable amount of sediment to be transported, leading to the severe erosion of each dam. It is also seen that dams located upstream are eroded more severely, but that more deposition occurs at downstream dams. This is because landslide dams 'inherently' prevent flow propagation, and the overall peak energy decreases along the channel, but the entrainment of sediment material leads to the flow growth. A number of studies have identified the important role of sediment entrainment in momentum growth along the flow movement. For example, based on flume experiments, Iverson et al. (2011) found that entrainment is accompanied by increased flow momentum and speed in wet bed sediments by facilitating progressive bed scour, reducing basal friction, and instigating positive feedback. Similar findings were reported by Guan et al. (2015; 2016a) through numerical modeling of a real-world flash flood event. Iverson et al. (2011) also indicated that the entrainment to flow of dryer bed sediment causes negative feedback and decreases flow momentum. This explains the physical phenomenon of the decreased flow speed at the initial stage but increased velocity downstream for the movable scenario in Figure 8(b). For the presence of a cluster of natural dams in a steep channel, this study has found that the bulk effects of sediment entrainment result in the overall flow growth in terms of peak depth, peak velocity, and peak discharge, which is consistent with previous findings. However, fluctuation occurs during the overall flow amplification along the channel and it depends on the location of natural dams. Figure 9 shows that the key flow variables decrease at the upslope region of each dam. However, any dam failure will enable the flow to have a sharp growth downstream of the dam; the blockage effect is more significant for larger-sized dams, yet the flow growth in case of their failure is also more remarkable (Figure 9 and 10). This is because landslide dam failure is a physical process of flow energy conversion; reservation of flow depth implies destructive power after sudden release. The flow growth characteristics shown in Figure 9 and 10 have been also reported

by some studies based on experimental investigations with different scales (e.g. Xue et al., 2011; Zhou et al., 2012; Niu et al., 2012). However, these studies provided only limited data from scarce monitoring points, rather than detailed hydraulic changes along the channel. For example, although the amplification effect along the channel has been emphasized, the increasing trend is not linear, but rather fluctuating with first a decrease and then an increase. Moreover, little attention has been paid to the effects of landslide dam size on flood dynamics, which is an important consideration. All these behaviors are well described with modeled dynamic evidence in this study.

4.3.*The impact of channel bend on flow evolution*

The bend feature of a channel is known to push the flow towards the outer bank slide, thereby driving more sediment to be entrained there (Palmsten et al., 2015; Guan et al., 2016b). The resultant flow feature will certainly influence the evolution of flash flooding when meeting with a cluster of landslide dams. However, although its effect has been recognized (Zhou et al., 2015; Itoh et al., 2018), none of the previous studies have examined how the bend feature exactly affects the growth of the flow along a sloping channel. It is seen that in a bend channel, flash flooding grows overall in size and speed as sediment materials are entrained, which is similar to the process in a straight channel. However, the flow velocity grows more significantly after flowing through convex-side dams (dam 1 and 3 in Figure 11(b)), because the value of the velocity profile in a bend channel is larger in the outer bank side than in the inner bank side. Nonetheless, the flow discharge grows faster after passing through concave-side dams (dam 2 and 4 in Figure 11(c)). A key reason is that the availability of sediment material for entrainment is smaller for dam 1 and 3, thus leading to a smaller growth of flow volume.

5. CONCLUSION

This study systematically investigates spatio-temporal dynamic processes of flash flooding over a sloping channel with a cluster of natural landslide dams based on numerical simulations. Conclusions drawn include the following key points. (1) A cascading dam failure is a highly unsteady process of water and sediment transportation, and peak depth is usually not equal to the difference between the peak level and final bed elevation (field depth). Traditional evaluation of the peak discharge using the field depth may generate large errors. (2) The hydraulic parameters, such as peak depth, velocity, and discharge, are amplified by the downstream natural landslide dams and bed erosion because of the bulk effects of sediment entrainment. The amplification mode varies with the location of the natural landslide dams. Peak depth and peak discharge increase at both sides of the dams; peak velocity first reduces at the upstream side and remarkably rises at the downstream side; and peak energy is shown to decrease moderately at the upstream side and fall sharply at the downstream side of the dam. (3) A bigger-sized landslide dam prevents flash flooding better by slowing down the wave speed, but it raises the potential energy of the flow at the upstream of the dam. That implies the potential risk in case of 'sudden-onset' dam failure. (4) Although similar amplification effects due to a cascading failure of natural dams are found, the physical characteristics of the bend channel alter the magnitude of flood hydrodynamic influence due to dam failure along the channel. Natural landslide dams in the convex side play a stronger role in amplifying peak

flow depth, velocity, and energy, but the failure of dams in the concave side increases peak discharge more significantly. This implies the complexity of the cascading hydraulics of natural landslide dam failure in real-world situations. In light of the lack of detailed spatio-temporal dynamic data from both laboratory experiments and field investigations, this study designs comprehensive scenarios and uses an advanced hydro-morphodynamic model to develop understanding of cascading failures of landslide dams in steep sloping channels. Both the model developed and the conclusions drawn can support the formation of risk prevention strategies for flash flooding in mountainous areas.

Author Contribution

Qingyuan Yang: Methodology, Validation, Formal analysis, Writing – Original Draft; *Mingfu Guan*: Supervision, Funding Acquisition, Conceptualization, Methodology, Formal Analysis, Writing – Review and Editing; *Yong Peng*: Conceptualization, Writing – Review and Editing; *Huayong Chen*: Data Curation, Writing – Review and Editing.

ACKNOWLEDGEMENTS

The work is supported by Grants (Grant No. 51909227 and 51609014) from the National Natural Science Foundation of China, and Seed Funding from the University of Hong Kong (Grant No. 201812159002).

REFERENCES

Bai, Y.C., Xu, D. and Lu, D.Q., 2007. Numerical simulation of two-dimensional dam-break flows in curved channels, Journal of Hydrodynamics, Ser. B, 19(6), 726-735.

Berger, C., McArdell, B. W., Fritschi, B. and Schlunegger, F. A., 2010. Novel method for measuring the timing of bed erosion during debris flows and floods. Water Resources Research, 46, W02502.

Bohorquez, P., Jimenez-Ruiz, P.J. and Carling, P.A., 2019a. Revisiting the dynamics of catastrophic late Pleistocene glacial-lake drainage, Altai Mountains, central Asia. Earth-Science Reviews, 197, 102892.

Bohorquez, P., Cañada-Pereira, P., Jimenez-Ruiz, P.J. and del Moral-Erencia, J.D., 2019b. The fascination of a shallow-water theory for the formation of megaflood-scale dunes and antidunes. Earth-Science Reviews, 193, 91-108.

Cao, Z., Pender, G., Wallis, S. and Carling, P., 2004. Computational dam-break hydraulics over erodible sediment bed. Journal of Hydraulic Engineering, 130(7), 689-703.

Cao, Z., Yue, Z. and Pender, G., 2011a. Landslide dam failure and flood hydraulics. Part I: Experimental investigation. Natural hazards, 59(2), 1003-1019.

Cao, Z., Yue, Z. and Pender, G., 2011b. Landslide dam failure and flood hydraulics. Part II: Coupled mathematical modelling. Natural Hazards, 59(2), 1021-1045.

Chen, H.Y., Cui, P., Zhou, G.D., Zhu, X.H. and Tang, J.B., 2014. Experimental study of debris flow caused by domino failures of landslide dams. International Journal of Sediment Research, 29(3), 414-422.

Chen, S.C., Lin, T.W. and Chen, C.Y., 2015. Modeling of natural dam failure modes and downstream riverbed morphological changes with different dam materials in a flume test. Engineering Geology, 188, 148-158.

Coleman, S. E., Andrews, D. P. and Webby, M. G. 2002. Overtopping breaching of noncohesive homogeneous embankments. Journal of Hydraulic Engineering, 128(9), 829-838.

Costa, J.E. and Schuster, R.L., 1988. The formation and failure of natural dams. Geological Society of America Bulletin, 100(7), 1054-1068.

Cui, P., Zhu, Y.Y., Han, Y.S., Chen, X.Q. and Zhuang, J.Q., 2009. The 12 May Wenchuan earthquake-induced landslide lakes: Distribution and preliminary risk evaluation. Landslides, 6(3), 209-223.

Cui, P., Zhou, G.D., Zhu, X.H. and Zhang, J.Q., 2013. Scale amplification of natural debris flows caused by cascading landslide dam failures. Geomorphology, 182, 173–189.

Dijkstra TA, Chandler JH, Wackrow R, Meng XM, Ma DT, Gibson A., et al., 2012. Geomorphic controls and debris flows – The 2010 Zhouqu disaster, China. In Eberhardt E, Froese C, Turner K, Leroueil S, editors, Landslides and Engineered Slopes: Protecting Society through Improved Understanding : Proceedings of the 11th International Symposium on Landslides and 2nd North American Symposium on Landslides. 1 ed. Vol. 1. Banff: CRC Press Inc. 2012.

Di Cristo, C., Evangelista, S., Greco, M., Iervolino, M., Leopardi, A. and Vacca, A., 2018. Dam-break waves over an erodible embankment: Experiments and simulations. Journal of Hydraulic Research, 56(2), 196-210.

Ermini, L. and Casagli, N., 2003. Prediction of the behavior of landslide dams using a geomorphological dimensionless index. Earth Surface Processes and Landforms: The Journal of the British Geomorphological Research Group, 28(1), 31-47.

Fan, X.M., van Westen, C.J., Xu, Q., Gorum, T., Dai, F., Wang, G. and Huang, R., 2013. Spatial distribution of landslide dams triggered by the 2008 Wenchuan Earthquake. Landslide Science and Practice, 5, 279-285.

Ferreira, R.M.L., Franca, M.J., Leal, J.G.A.B. and Cardoso, A.H., 2009. Mathematical modelling of shallow flows: Closure models drawn from grain-scale mechanics of sediment transport and flow hydrodynamics. Canadian Journal of Civil Engineering, 36(10), 1605-1621.

Guan, M., Wright, N.G. and Sleigh, P.A., 2014. 2D process-based morphodynamic model for flooding by noncohesive dyke breach. Journal of Hydraulic Engineering, 140(7), p.04014022.

Guan, M., Wright, N.G., Sleigh, P.A. and Carrivick, J.L., 2015. Assessment of hydro-morphodynamic modelling and geomorphological impacts of a sediment-charged jökulhlaup, at Sólheimajökull, Iceland. Journal of Hydrology, 530, 336-349.

Guan, M., Carrivick, J.L., Wright, N.G., Sleigh, P.A. and Staines, K.E., 2016a. Quantifying the combined effects of multiple extreme floods on river channel geometry and on flood hazards. Journal of Hydrology, 538, 256-268.

Guan, M., Wright, N.G. , Sleigh, P. A., Ahilan, S. and Lamb, R., 2016b. Physical complexity to model morphological changes at a natural channel bend, Water Resources Research, 52, 6348–6364.

Itoh, T., Ikeda, A., Nagayama, T. and Mizuyama, T., 2018. Hydraulic model tests for propagation of flow and sediment in floods due to breaking of a natural landslide dam during a mountainous torrent. International Journal of Sediment Research, 33(2), 107-116.

Iverson, R., Reid, M., Logan, M. et al., 2011. Positive feedback and momentum growth during debris-flow entrainment of wet bed sediment. Nature Geoscience, 4, 116-121.

Iverson, R.M., and Ouyang, C., 2015, Entrainment of bed material by Earth-surface mass flows: review and reformulation of depth-integrated theory, Reviews of Geophysics, 53, 27-58.

Jiang, X.G., Wei, Y.W., Wu, L. and Lei, Y., 2018. Experimental investigation of failure modes and breaching characteristics of natural dams, Geomatics, Natural Hazards and Risk, 9(1), 33-48

Korup, O., Densmore, A.L. and Schlunegger, F., 2010. The role of landslides in mountain range evolution. Geomorphology, 120(1-2), 77-90.

Liao, H.M., Yang, X.G., Tao, J. and Zhou, J.W., 2019. Experimental study on the river blockage and landslide dam formation induced by rock slides. Engineering Geology, 261, 105269.

Miller S. and Chaudhry, M.H., 1989. Dam-break flows in curved channel. Journal of Hydraulic Engineering, 115(11), 1465-1478.

Morris, M.W., Hassan, M. and Vaskinn, K.A. 2007. Breach formation: Field test and laboratory experiments. Journal of Hydraulic Research, 45, 9-17.

Niu, Z.P., Xu, W.L. and Li, N.W., 2012. Experimental investigation of the failure of cascade landslide dams. Journal of Hydrodynamics, 24(3), 430-441.

Palmsten, M.L., Kozarek, J.L. and Calantoni, J., 2015. Video observations of bed form morphodynamics in a meander bend, Water Resources Research, 51, 7238-7257.

Peng, M., Zhang, L.M., Chang, D.S. and Shi, Z.M., 2014. Engineering risk mitigation measures for the landslide dams induced by the 2008 Wenchuan earthquake. Engineering Geology, 180, 68-84.

Pugh, F.J. and Wilson, K.C., 1999. Velocity and concentration distributions in sheet flow above plane beds. Journal of Hydraulic Engineering, 125(2), 117-125.

Schmocker, L. and Hager W.H., 2010. Overtopping and breaching of dikes – Breach profile and breach flow. oc. International Conference in River Flow, A. Dittrich, K. Koll, J. Aberle, P. Gei-senhainer, eds., Braunschweig, Germany, 515-522.

Schuster, R.L., 1986. Landslide Dams: Processes, Risk, and Mitigation. New York, NY. ASCE.

Shi, Z.M., Guan, S.G., Peng, M., Zhang, L.M. et al., 2015. Cascading breaching of the Tangjiashan landslide dam and two smaller downstream landslide dams. Engineering Geology, 193, 445-458.

Soulsby, R.L., 1997. Dynamics of Marine Sands. London, UK. Thomas Telford.

Staines, K.E.H., Carrivick, J.L., 2015. Geomorphological impact and morphodynamic effects on flow conveyance of the 1999 jökulhlaup at sólheimajökull, Iceland. Earth Surf. Process. Landforms, 40(10), 1401-1416.

Tang, C., Rengers, N., Van Asch, T.W.J., Yang, Y.H. and Wang, G.F., 2011. Triggering conditions and depositional characteristics of a disastrous debris flow event in Zhouqu city, Gansu Province, northwestern China. Natural Hazards and Earth System Science, 11(11), 2903-2912.

Walder, J.S. and O'Connor, J.E. (1997). Methods for predicting peak discharge of floods caused by failure of natural and constructed earthen dams. Water Resources Research, 33(10), 2337-2348.

Wang, F., Dai, Z., Okeke, C.A.U., Mitani, Y. and Yang, H., 2018. Experimental study to identify premonitory factors of landslide dam failures. Engineering Geology, 232, 123-134.

Wang, L., Chen, Z., Wang, N., Sun, P., Yu, S., Li, S. and Du, X., 2016. Modeling lateral enlargement in dam breaches using slope stability analysis based on circular slip mode. Engineering Geology, 209, 70-81.

Weidner, L., DePrekel, K., Oommen, T. and Vitton, S., 2019. Investigating large landslides along a river valley using combined physical, statistical, and hydrologic modeling. Engineering Geology, 259, 105169.

Wong, M. and Parker, G., 2006. Reanalysis and correction of bed-load relation of Meyer-Peter and Müller using their own database. Journal of Hydraulic Engineering, 132(11), 1159-1168.

Wu, W. and Wang, S.S., 2007. One-dimensional modeling of dam-break flow over movable beds. Journal of Hydraulic Engineering, 133(1), 48-58.

Xue, Y., Xu, W.L., Luo, S.J. et al., 2011. Experimental study of dam-break flow in cascade reservoirs with steep bottom slop. Journal of Hydrodynamics-Ser. B, 23(4), 491-497.

Zhou, G. D., Cui, P., Chen, H.Y., Zhu, X. et al., 2012. Experimental study on cascading landslide dam failures by upstream flows. Landslides, 10, 633-643.

Zhou, G. D., Cui, P., Zhu, X., Tang, J., Chen, H. and Sun, Q., 2015. A preliminary study of the failure mechanisms of cascading landslide dams. International Journal of Sediment Research, 30(3), 223-234.

Zhou, G. D., Zhou, M., Shrestha, M. S. et al., 2019. Experimental investigation on the longitudinal evolution of landslide dam breaching and outburst floods. Geomorphology, 334, 29-43.